# Laser Doppler imaging, revisited

Michael Atlan, Michel Gross

# Laser Doppler imaging, revisited

M. Atlan, M. Gross

*Laboratoire Kastler-Brossel, UMR 8552 (ENS, CNRS, UMPC), Ecole Normale Supérieure, 10 rue Lhomond F-75231 Paris cedex 05*

We present a detection scheme designed to perform laser Doppler imaging in a wide-field configuration, aimed at slow flows characterization. The optical field which carries a spectral information about the local scatterers dynamic state that results from momentum transfer at each scattering event, is analyzed in the temporal frequencies domain. The setup is based on heterodyne off-axis digital holography.

The imaging technique presented here is a laser Doppler scheme in an off-axis holographic configuration. A heterodyne optical mixing configuration on a CCD camera is used to select and enhance a tunable frequency component of the probe light to measure its Doppler linewidth. Holography is an established scheme in particle field diagnosis (13) and velocimetry (14; 16). Off-axis holographic particle velocimetry (HPV) was reported to be superior to inline HPV in terms of signal-to-noise ratio (SNR) (8) and is the subject of recent developments (9). We intend to demonstrate that off-axis holography is also a valuable candidate for laser Doppler linewidth measurements, which are demanding in terms of SNR. In conventional laser Doppler velocimetry (LDV), scattered light coming from a point focused onto a sample is detected by a single detector and analyzed by a spectrum analyzer. The power spectrum of coherent monochromatic light scattered by moving particles is broadened as a result of momentum transfer. The Doppler shift for one scattering event is (18) :

$$\omega_D = (\mathbf{k_s} - \mathbf{k_i}) \cdot \mathbf{v} \qquad (1)$$

where $\mathbf{k_i}$ is the incident wave vector, $\mathbf{k_s}$ the scattered wave vector and $\mathbf{v}$ the scatterer instantaneous velocity. The resulting broadening of light is linked to the velocity distribution of scatterers (1; 3). The detection sensitivity can be improved by homodyne or heterodyne amplification which consists in mixing scattered light with a local oscillator (LO) (4). Doppler maps can be realized by scanning the focus point on the sample surface, which constitutes the principle of scanning laser Doppler Imaging (LDI). The instrument presented here uses an optical heterodyne mixing scheme on an array detector to perform quantitative, parallel, wide-field LDI. Contrarily to Fourier transform spectroscopy schemes, the measurement is done directly in the temporal frequency domain by detuning the LO frequency and measuring one spectral point at a time.

The experimental setup is based on an optical interferometer sketched in fig. 1(a). A CW, 80 mW, 780 nm Sanyo DL-7140-201 diode provides the main laser beam (field $E_\mathrm{L}$, angular frequency $\omega_\mathrm{L}$). A small part of this beam is split by a prism to form a reference beam (local oscillator, LO), while the remaining part is expanded

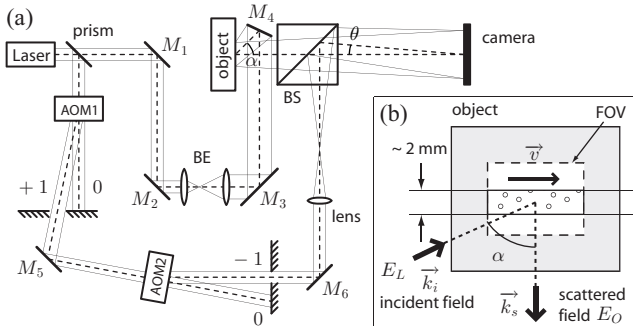


FIG. 1 (a) Setup. $M_1$ to $M_6$: mirrors; BS: beam splitter; BE: beam expander; AOM1 , AOM2: acousto-optic modulators (Bragg cells); -1, 0, +1 : diffraction orders. (b) object and optical configuration. FOV: field of view. $\alpha$: scattering angle. $\mathbf{v}$ : flow direction. $\mathbf{k_i}$: incident wave vector. $\mathbf{k_s}$: scattered wave vector, in the direction of the receiver. $E_L$: laser (incident) field. $E_\mathrm{O}$: field scattered by the object. $E_\mathrm{LO}$: reference (local oscillator) field.

and illuminates the object with an average incidence angle $\alpha$. The field scattered by the object, $E_\mathrm{O}$, is mixed with the LO field $E_\mathrm{LO}$ and detected by a PCO PixelFly 1.3 Megapixel CCD camera (square pixels, pixel size: 6.7 $\mu$m, framerate $\omega_S/2\pi = 8\,\mathrm{Hz}$), set at a distance $d =$ 50 cm from the object. Two Bragg cells (acousto-optic modulators, AOM, Crystal Technology) are used to shift the LO by a tunable frequency. A 10 mm focal length lens is placed in the reference arm in order to create an off-axis ($\theta \approx 1°$ tilt angle) virtual point source in the object plane (see fig. 1(a)). This configuration constitutes a lensless Fourier holographic setup (12).

To perform an heterodyne detection of the component of the object field at frequency $\omega = \omega_\mathrm{L} + \Delta\omega$, the LO field $E_\mathrm{LO}$ is adjusted at frequency $\omega_\mathrm{LO} = \omega_\mathrm{L} + \Delta\omega - \omega_\mathrm{S}/n$ with $n > 2$ (typically $n = 4$). The $\Delta\omega$ shift allows the LO field to match the part of the object field shifted by $\Delta\omega$ (i.e. their combination produces a static interference pattern), while the additional shift $\omega_\mathrm{S}/n$ provokes a modulation of the interference pattern at $\omega_\mathrm{S}/n$, which is slow enough to be sampled by the CCD camera (the beat frequency $\omega_\mathrm{S}/n$ fulfil the sampling theorem condition $\omega_\mathrm{S}/n < \omega_\mathrm{S}/2$).

The incident (laser) field is noted:

$$E_{\mathrm{L}}(t) = E_{\mathrm{L}}(\omega_{\mathrm{L}}) \exp(i\omega_{\mathrm{L}} t) \quad (2)$$

The part of the scattered (object) field shifted at $\omega$ (as a consequence of momentum transfer), is:

$$E_{\mathrm{O}}(t) = E_{\mathrm{O}}(\omega_{\mathrm{L}} + \Delta\omega) \exp\left[i(\omega_{\mathrm{L}} + \Delta\omega)t\right] \quad (3)$$

The LO field is :

$$E_{\mathrm{LO}}(t) = E_{\mathrm{LO}}(\omega_{\mathrm{L}} + \Delta\omega - \frac{\omega_{\mathrm{S}}}{n}) \times \exp\left[i(\omega_{\mathrm{L}} + \Delta\omega - \frac{\omega_{\mathrm{S}}}{n})t\right] \quad (4)$$

The intensity $I$ detected by the camera can be expressed as a function of the complex fields (2) :

$$I(t) = \left|E_{\mathrm{O}}(t) + E_{\mathrm{LO}}(t)\right|^2 \quad (5)$$

The part of $I$ modulated at $\omega_{\mathrm{S}}/n$ (also called heterodyne term) takes the following form:

$$I_{\frac{\omega_{\mathrm{S}}}{n}} = E^*_{\mathrm{LO}}(\omega_{\mathrm{L}}+\Delta\omega-\frac{\omega_{\mathrm{S}}}{n}) E_{\mathrm{O}}(\omega_{\mathrm{L}}+\Delta\omega) \exp(i\omega_{\mathrm{S}} t/n) \quad (6)$$

Note that the LO field amplitude can be considered as constant in the range of frequency shifts of this study ($|\Delta\omega| < 2\,\mathrm{kHz}$). Let's define $A = \left|E_{\mathrm{LO}}(\omega_L + \Delta\omega - \omega_{\mathrm{S}}/n)\right|^2$. The complex amplitude of the considered heterodyne term $E^*_{\mathrm{LO}}(\omega_{\mathrm{L}} + \Delta\omega - \omega_{\mathrm{S}}/n) E_{\mathrm{O}}(\omega_{\mathrm{L}} + \Delta\omega)$ constitutes the *heterodyned* object field distribution (OFD). Its power $S$ is:

$$S(\Delta\omega) = A \left|E_{\mathrm{O}}(\omega_{\mathrm{L}} + \Delta\omega)\right|^2 \quad (7)$$

This quantity is read-out from a sequence of $n$ images recorded by the camera. The squared amplitude of the $\omega_{\mathrm{S}}/n$ frequency component of $I(t)$, calculated by a numerical Fourier transform of the $n$-image sequence, is proportional to $S(\Delta\omega)$. The modulation/demodulation scheme, described here, is based on the frequency-shifting technique (7). It is the dynamic equivalent of the phase-shifting digital holography technique (10; 17). The lensless Fourier holographic setup (12) is less demanding in numerical calculations than the general Fresnel holography configuration. The numerical reconstruction algorithm of the image is limited to one discrete Fourier transform (11; 15). The artefacts due to the finite size of the sensor and the spatial discrete Fourier transform are narrower than one pixel in the reconstructed image (6), and hence can be neglected.

$S(\Delta\omega)$ is proportional to the spectral power density of the signal field integrated in the frequency window $\Delta\omega \pm \omega_{\mathrm{S}}/2n$. We define the signal $S_{\mathrm{dB}}$ represented on spectra profiles and spatial maps as :

$$S_{\mathrm{dB}}(\Delta\omega) = 10 \log_{10}\left[\frac{S(\Delta\omega)}{N(\Delta\omega)}\right] \quad (8)$$

where $N(\Delta\omega)$ is the quantity $S(\Delta\omega)$ assessed in a region of the reconstructed hologram where the object light contribution is null. It was reported to be close to shot-noise (5).

The sample designed for the experiment consists in a $\sim$ 2 mm-wide canal carved out from a 127 $\mu$m parafilm (TM) layer sandwiched between two 1 mm-thick coverglasses (see fig. 1(b)). This sample was set in front of a white sheet of paper, used to scatter incident light in the direction of the detector. A 1.5% volumic concentration aqueous suspension of latex beads of 1.04 $\mu$m of diameter, is perfused in the sample with constant flow thanks to a motorized syringe. A Mie algorithm [1] was used to assess its optical parameters : the scattering coefficient is $\mu_s = 43.6\,\mathrm{mm}^{-1}$, and the anisotropy coefficient is $g = 0.9$. The suspension of latex beads was perfused through the canal of the first sample at several flow rates. The average incidence angle $\alpha$ of the laser beam (see fig. 1(b)) is $\sim 45°$. In this experiment, $S(\Delta\omega)$ maps were realized for $\Delta\omega$ in the [-2.048 kHz, +2.048 kHz] range with $n = 4$ and spacing interval of 8 Hz. $S(\Delta\omega)$ was averaged over $m$ images for each frequency point. One whole spectral cube measurement took $\sim$ 8 minutes and 30 seconds (= 8 images $\times$ 513 frequency shifts $\times$ 1/8 second exposure time), and one spectral point was acquired in 1 second. A steady flow was thus required here for the chosen span and spacing of measured Doppler shifts.

In fig. 2a, the detection is tuned far enough ($\Delta\omega/(2\pi) = -2.048\,\mathrm{kHz}$) where neither statically nor dynamically scattered light should be observed, to measure the noise contribution ($< 1\,\mathrm{dB}$). In fig. 2b, the detection is tuned at the maximum of the Doppler shifted and broadened light distribution $\Delta\omega/(2\pi) = -304\,\mathrm{Hz}$ (see fig. 3 c). In fig. 2c, the detection is tuned at a small frequency shift ($\Delta\omega/(2\pi) = -8\,\mathrm{Hz}$) to map very slow velocities. This map reveals an exaltation of small velocities at the border of the canal region, in the absence of any wetting layer. In fig. 2d, the detection is tuned at null frequency shift ($\Delta\omega/(2\pi) = 0\,\mathrm{Hz}$) to measure backscattered light ($\sim 16\,\mathrm{dB}$) from the static background.

Spectra were calculated in two different regions of the image. The background area and the canal area. The spectrum of light scattered by the background produces the tight peak centered at null frequency shift (fig. 3(a)). It can be interpreted as a measurement of the instrumental linewidth. In the canal area spectra at three flow rates were realized: the first flow rate was null (fig. 3(b)). The observed symmetric spectral broadening is attributed to brownian motion of the latex particles. The second flow rate was $2.2 \times 10^{-4}\,\mathrm{ml.s}^{-1}$, which would correspond to a uniform particle velocity

[1] `http://omlc.ogi.edu/calc/mie_calc.html`

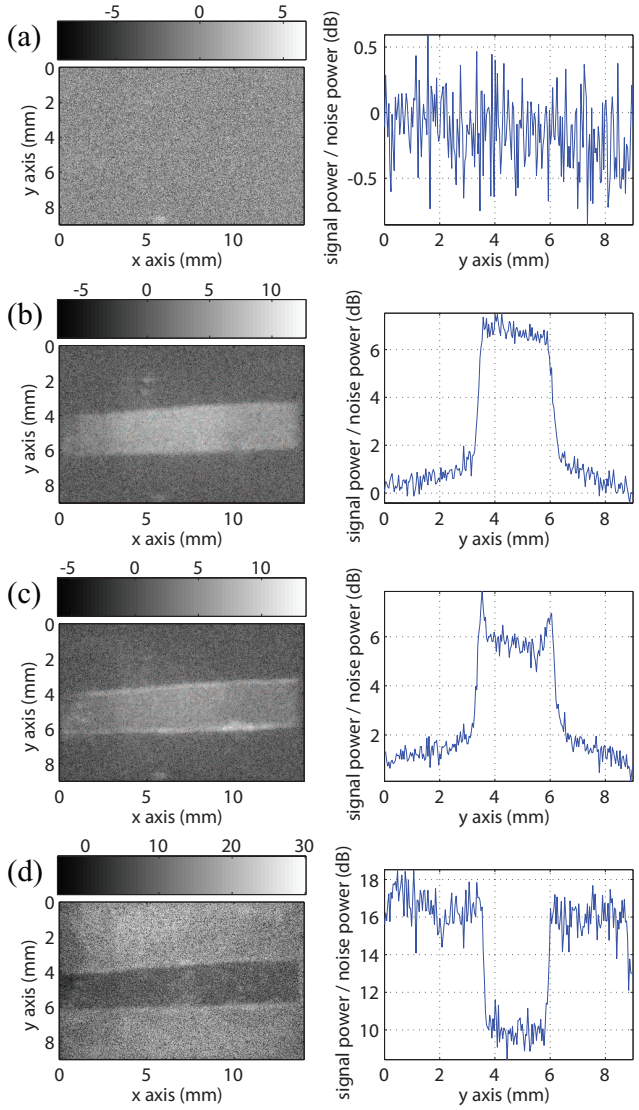


FIG. 2 Results obtained with the sample perfused with average velocity $v_1$. Left: $S_{\mathrm{dB}}(\Delta\omega)$ Right : profiles at $x = 8$ mm. (a) $\Delta\omega/(2\pi) = -2.048\,\mathrm{kHz}$. (b) $\Delta\omega/(2\pi) = -304\,\mathrm{Hz}$. (c) $\Delta\omega/(2\pi) = -8\,\mathrm{Hz}$. (d) $\Delta\omega/(2\pi) = 0\,\mathrm{Hz}$.

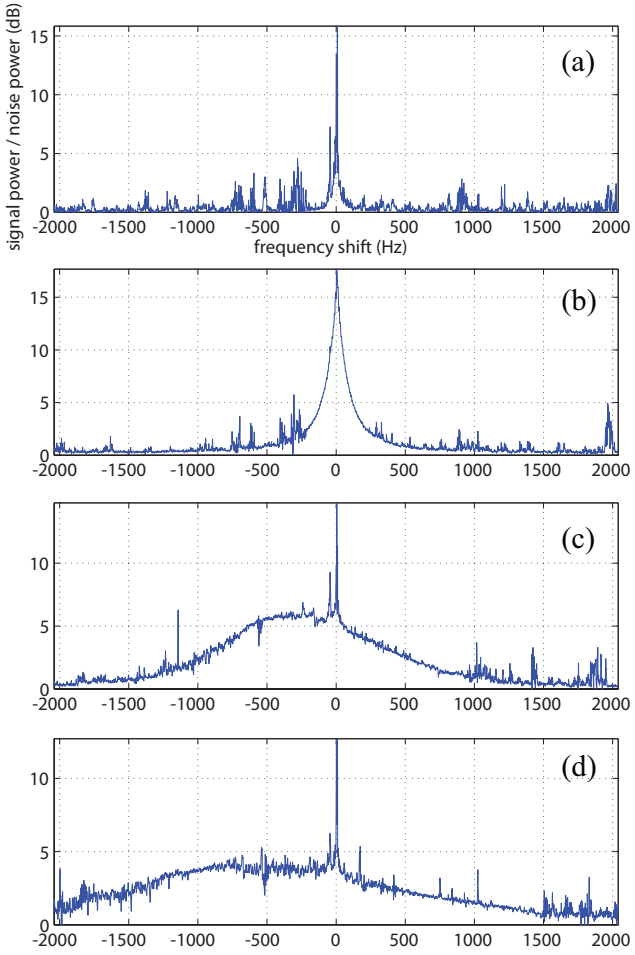


FIG. 3 (a) $S_{\mathrm{dB}}$ spectrum of the static background region (frequency-domain instrumental response function). (b, c, d) $S_{\mathrm{dB}}$ average spectra in the canal region. (b) Null average velocity. (c) $v = v_1$. (d) $v = v_2 = 2v_1$

$v_1 = 870\,\mu\mathrm{m.s}^{-1}$. The corresponding spectrum is represented on fig. 3(c). The full width at half maximum (-3 dB) of the Doppler peak is $\sim$ 1500 Hz. The third flow rate was $4.4 \times 10^{-4}\,\mathrm{ml.s}^{-1}$, which would correspond to a uniform particle velocity of $v_2 = 1.74\,\mathrm{mm.s}^{-1}$. The corresponding spectrum is represented on fig. 3(d), which shows a broader Doppler peak than in the previous case. Note that we were unable to measure spectral signatures beyond $\pm 2$ kHz. This suggests an intrinsic restriction of the presented instrument to the characterization of small flows.

In conclusion, the presented setup performs a parallel measurement of the power spectrum of scattered monochromatic light. The presented scheme is different from conventional time-domain measurements. Basically, each pixel on a camera acts as an heterodyne photodetector that samples Doppler-shifted light. Each frequency point of the spectrum is acquired at a time, by detuning the LO frequency. The frequency resolution is given by the heterodyne bandwidth of the detection (the inverse of the acquisition time of the $n$-image sequence), hence the potential suitability for microflow diagnosis (bioflow, microfluidics). Furthermore, the optical configuration allows one to measure algebraic Doppler shifts since we can spatially discriminate the two heterodyne terms in the recorded hologram.

*We are grateful to Claude Boccara and Jacques Dufaux for their constant interest since the earliest stages of the development of this instrument.* Contact : atlan@lkb.ens.fr

## References


[1] R. Bonner and R. Nossal. *Applied Optics*, 20:2097–2107, 1981.

[2] M. Born and E. Wolf. Pergamon Press, 6 edition, 1993.

[3] J. A. Briers. *JOSA A.*, 13:345, 1996.

[4] R. Brown. *Applied Optics*, 40:4004, 2001.

[5] M. Gross, P. Goy, and M. Al-Koussa. *Optics Letters*, 28:2482–2484, 2003.

[6] Thomas M. Kreis. *Optical Engineering*, 41(4):771–778, 2002.

[7] F. LeClerc, L. Collot, and M. Gross. *Optics Letters*, 25(10):716–718, 2000.

[8] H Meng and F Hussain. *Appl. Opt.* , 34:1827–+, April 1995.

[9] Hui Meng, Gang Pan, Ye Pu, and Scott H Woodward. *Measurement Science and Technology*, 15(4):673–685, 2004.

[10] U. Schnars and W. Juptner. *Appl. Opt.*, 33:179–181, 1994.

[11] U. Schnars and W. P. O. Juptner. *Meas. Sci. Technol.*, 13:R85–R101, 2002.

[12] George W. Stroke. *Applied Physics Letters*, 6(10):201–203, 1965.

[13] BJ Thompson, JH Ward, and WR Zinky. *Applied Optics*, 6(3):519, 1967.

[14] JD Trolinger, RA Belz, and WM Farmer. *Appl. Opt.*, 8(5):957, 1969.

[15] Christoph Wagner, Sonke Seebacher, Wolfgang Osten, and Werner Juptner. *Applied Optics*, 38:4812–4820, 1999.

[16] LM Weinstein, GB Beeler, and AM Lindemann. *American Institute of Aeronautics and Astronautics*, AIAA-526, 1985.

[17] I. Yamaguchi and T. Zhang. *Optics Letters*, 18:31, 1997.

[18] Y. Yeh and H. Z. Cummins. *Appl. Phys. Lett.*, 4:176–179, 1964.